Visualization of Ethyl Alcohol Droplet Breakup with Large Deformations in a Continuously Accelerated Flow Field

Suthyvann Sor[1], Adelaida García-Magariño*[1], Pablo López[2] and Ángel Velazquez[2]

[1]Instituto Nacional de Técnica Aeroespacial (INTA), 28850 Torrejón de Ardoz, Spain
[2]Universidad Politécnica de Madrid (UPM), Madrid, Spain
*Corresponding author: garciamga@inta.es

Abstract

Droplets in a continuously accelerated flow field, under certain conditions, deform as oblate spheroids and breakup. This type of flow field differs from the traditional shock tube experiments where droplets are suddenly exposed to a constant high velocity airstream. Bag, bag and stamen and shear breakup were encountered in previous works for water droplets under these conditions. The aim of this investigation is the visualization of the breakup modes of ethyl alcohol droplets in a continuously accelerated flow field. In order to generate this continuously accelerating flow field allowing for the illumination, the rotating arm facility at INTA is used. In this facility, droplets were allowed to fall in the path of an incoming aerofoil of a chord of 1050 mm mounted at the end of a rotating arm and moving at velocities up to 60m/s. A high-speed camera recording images up to 45 000 fps and shadowgraph illumination technique was employed. For some cases, direct illumination technique and a high-resolution camera has also been used in this investigation. Under certain conditions, these droplets deform and breakup before impinging on the aerofoil. The influence of the droplet diameter (between 0.5 mm and 1.5 mm) and the aerofoil velocity (30-60 m/s) were investigated. In particular, a new type of breakup has been encountered for ethyl alcohol droplets of 1mm of diameter. After the deformations as an oblate spheroid, a bulge appears in the front part as in bag and stamen and it resemble the shape of a hat. However, then, instead of forming the bag, all the rear part of the droplet seems to collapse inside the droplet and a stamen is formed in the rear part of the droplets that grows a high quantity. At the same time, the droplet front part layer seems to shear back.

Keywords

Droplet Breakup, Non-stationary Flow Field

Introduction

Droplets breakups due to a high air stream has been widely studied mainly in shock tube [1,2] or wind tunnels facilities [3-5], where these droplets are suddenly exposed to the air speed. In the Guildenbecher et al. [6] review on this field, attention was paid to the breakup morphology and a similar classification of breakup mode as the one found in Pilch and Erdman [8] was established: Vibrational breakup, Bag Breakup, Multimode (Bag and Stamen), Sheet Stripping (Sheet Thinning), and Catastrophic Breakup. Another comprehensible review is the one of Theofanous [7], which made a good discussion on the two main mechanisms leading to breakup: Rayleigh-Taylor piercing and shear-induced entrainment. However, these two reviews [6,7] cover data obtained in facilities where droplets are suddenly exposed to a high constant velocity air stream. On the contrary, the aim of this paper is to study droplets that are initially in a quiescent flow and then the air velocity starts to increase gradually with an acceleration that also increases, until the acceleration and the velocity reach values that allow for droplet breakup. The problem is therefore a non-stationary problem and transient effects need to be considered. Accelerating and decelerated non-uniform flow fields have been studied for non-deformable spheres [9,10], or droplets that are small enough to neglect deformation [11] and it has been proved to be a very complex problem since there still exist contradicting results (see introduction in Ref. [12]). Only recently, a numerical simulation study has been conducted on unsteady drag coefficient of deformable droplets [13], where authors propounded that drag coefficient is mainly affected by an unsteady term and to a lesser extent by the Weber number. In this context, some previous work of the authors [14-16] have addressed aerobreakup experimentally for droplets in a continuous accelerated flow field, but only for water droplets. Studies of aerobreakup of ethanol droplets have been also performed [17], but in a constant air stream. Therefore, the novelty of this work is to study the aerobreakup of ethyl alcohol droplets in a non-stationary flow.

Material and methods

The accelerating flow field was created by means of the rotatory arm installation at INTA, Spain. Figure 1 shows an image of the installation. An electric motor of 5 KW with a vertical axis is attached to a support structure. An arm of length 2.16 m is attached to the vertical axis of the motor, which can provide rotational speeds up to 310 rpm. The airfoil model is mounted at the end of the rotating arm obtaining model velocities up to 60 m/s. An in-house monosized droplet generator allowed a stream of ethyl alcohol droplets to fall in the path of the incoming

airfoil, while the high speed camera FOTRON SA4 recorded images at an acquisition velocity between 30000 fps and 45000 fps depending on the droplet size and the resolution (See Fig.1 on the left). The lens for the camera were AF Micro Nikkor 200mm 1:4D and droplets were illuminated from the back with a 3W LED. Three droplets sizes were chosen for this experiment and for each droplet size a different resolution and acquisition rate were chosen according to Table 1.
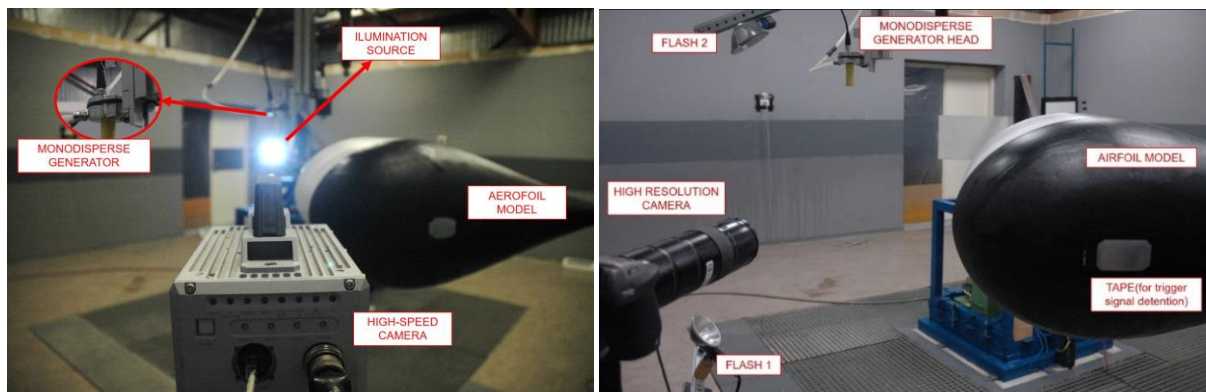

Figure 1. A photograph of the experimental setup during the tests. On the left shadowgraph technique is used while on the right direct illumination is employed.

Table 1. Experimental setup conditions.

Droplet Diameter (µm)	Resolution (H x V) (pix)	Acquisition Rate (fps)
500	256 x 285	40000
1000	192 x 304	45000
1500	192 x 480	30000

Additional tests for certain cases were also performed using the direct illumination technique previous presented by the authors [14]. An image of the experimental setup is shown in Fig. 1 on the right. Two flashes lamps, the 1538-A Strobotac Electronic Stroboscopic and the1539-A Stroboslave, illuminate the droplets (flash duration on the order of 3 µs), while images were recorded by the high resolution camera Hasselblad H3DII-39, which has a resolution of 7216 pixels (width) x 5412 pixels (height). The magnification was 151 pix/mm. The lens used were: HC 4/200 mm, two extensions H52 mm, and a converter H1.7x. The camera setup was ISO-800 and f/6.8. A LED trigger is placed at some point of the model pass and is able to detect the pass of the tape placed on the side of the model (see Fig. 1). The flashes are delayed a certain time from the trigger signal using a Programmable Timing Control Hub IDT. By choosing the delay time, the distance of the model to the droplets is varied.

x/chord	y/chord
1	0
0,937	0,014
0,877	0,028
0,818	0,044
0,762	0,059
0,707	0,076
0,655	0,093
0,604	0,11
0,556	0,127
0,51	0,143
0,465	0,158
0,423	0,171
0,383	0,183
0,344	0,192
0,308	0,198
0,274	0,2
0,241	0,2
0,211	0,196
0,183	0,191
0,157	0,183
0,133	0,173
0,11	0,162
0,09	0,15
0,072	0,136
0,056	0,121
0,042	0,105
0,03	0,089
0,02	0,072
0,012	0,055
0,006	0,041
0,002	0,022
0	0

Figure 2. Aerofoil model views on the left. Dimensionless coordinates of the airfoil profile on the right.

The airfoil model chosen, named as DBK004, has the same profile as previous used in these kind of studies [13-15] and a bigger chord (1.05 m). The airfoil model views and the dimensionless coordinates can be observed in Fig. 2. The model velocity was varied between 30 m/s and 60 m/s. The air velocity profile that the droplets would suffer as the model approaches them depending on the model velocity is displayed in Fig. 3 on the left where initially droplets were at a distance to the model of 500 mm. The air acceleration is displayed in Fig. 3 on the right, where it can be observed that as the model velocity increases the air acceleration also increases.
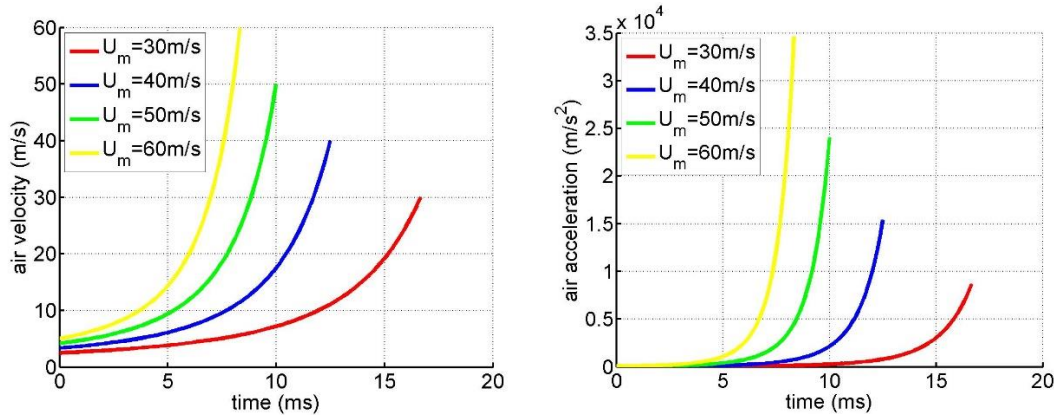
Figure 3. A photograph of the experimental setup during the tests.

Results and discussion

Three droplet sizes (D= 500 µm, D=1000 µm and D=1500 µm) and four model velocities (U_m=30 m/s, U_m=40 m/s, U_m=50 m/s and U_m=60 m/s) were tested. Table 2 shows the case key for each of the cases tested. However, droplet breakup evolution can not be observed in all the cases. For droplets of 500 µm of diameter, droplets deform as oblate spheroids and before any specific feature of the breakup type (i.e bag, bag and stamen, shear…) is observed droplets impinge on the airfoil. Therefore, the visualization of the evolution of these droplets does not provide new information and it is not presented here. Figure 4 shows the final deformation attained for these droplets for model velocities of 40 m/s (case #2), 50 m/s (case #3) and 60 m/s (case #4).

Table 2. Experimental matrix table.

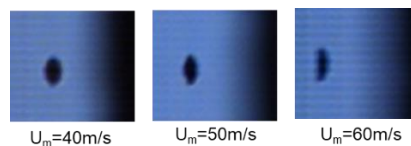| Case Key #	D = 500 µm	D = 1000 µm	D = 1500 µm
U_m = 30 m/s	1	5	9
U_m = 40 m/s	2	6	10
U_m = 50 m/s	3	7	11
U_m = 60 m/s	4	8	12

U_m=40m/s U_m=50m/s U_m=60m/s

Figure 4. Droplet final shape before impinging for droplets of 500 µm and model velocities of 40 m/s (on the left), 50 m/s (in the middle) and 60 m/s (on the right).

For droplets of diameter of 1000 µm and model velocity 30 m/s (case #5), droplets evolution is shown in Fig. 5. They deform as an oblate spheroid up to a point where a front bulge appears as in the traditional bag and stamen breakup type.

#762   #820   #850   #907   #921   #936   #944   #955   #959

Figure 5. Droplet Evolution Images. Run 100: Droplet Diameter 960µm, Model Velocity 30m/s. Corresponding frames are under each image. The acquisition rate was 45000 fps.

Figure 6 shows the droplet deformation and breakup evolution of a stream of droplets of 1000 µm while the airfoil model was moving at 40 m/s (case #6) using shadowgraph illumination technique. The model was approaching from the right, as observed in the last frame (frame #2072). The time from the beginning up to the last frame was 5 ms. It can be observed in Fig. 6 that a new type of breakup has been encountered. For a better visualization, some images using direct illumination technique were obtained and compared with shadowgraph images in Fig. 7. After the deformations as an oblate spheroid (frame #2029), a bulge appears in the front part as in bag and stamen and it resemble the shape of a hat pointing upstream (frame #2043). However, then, instead of forming the bag, all the rear part of the droplet seems to collapse inside the droplet (frame #2056) forming an inverted pyramid (frame #2064). Then the sharp end of the inverted pyramid become a rounded finger and the shape resembles a 'joystick' pointing downstream. This mechanism has not been observed in the traditional bag, bag and stamen or shear breakup. Therefore, a more detailed evolution of this mechanism is displayed in Fig. 8, where all the frames between frame #2045 to frame # 2069 are shown for the third droplet in Fig. 6. An evolution of the instantaneous Reynolds number (Re), instantaneous Weber number (We) and a relationship between characteristic time of droplet deformation, defined as $t_{dd} = \sqrt{\rho_{et}\pi D^3/(6\sigma)}$, and characteristic time of flow acceleration, $t_{fa} = U_{air}/\frac{dU\_air}{dt}$, can also be found at Fig. 7 .
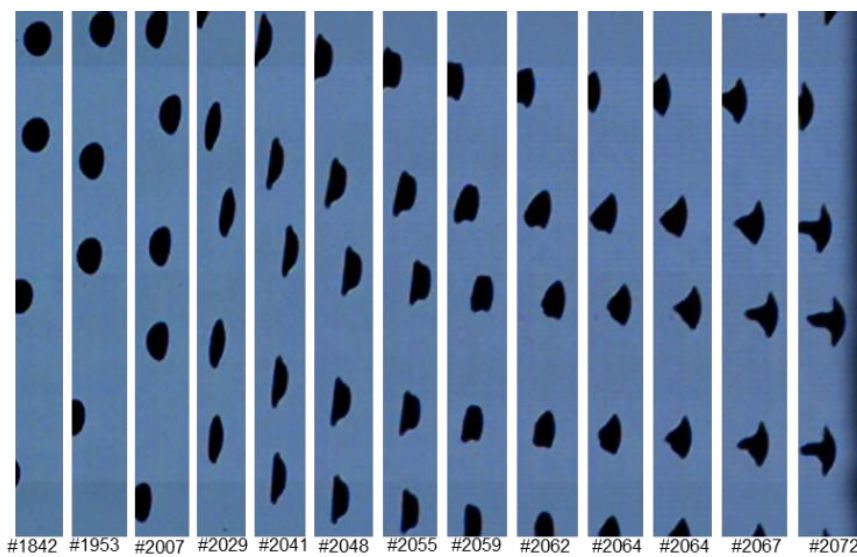

Figure 6. Droplet Evolution Images. Run 101: Droplet Diameter 1mm, Model Velocity 40m/s. Corresponding Frames are under each image. The acquisition rate was 45000 fps.
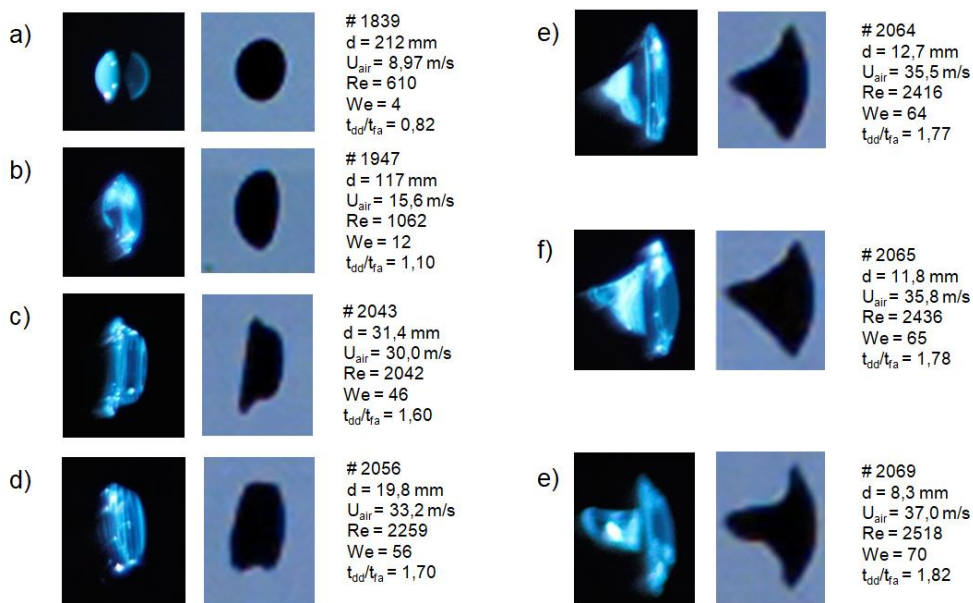

Figure 7. Droplet Evolution Images. Run 101: Droplet Diameter 1mm, Model Velocity 40m/s. Corresponding Frames are on the right of each image. The acquisition rate was 45000 fps.
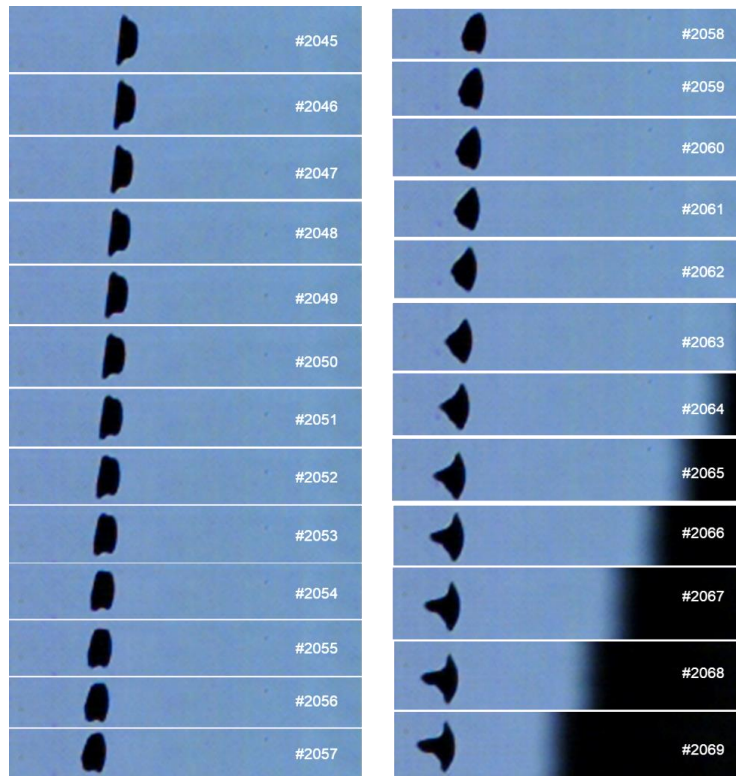
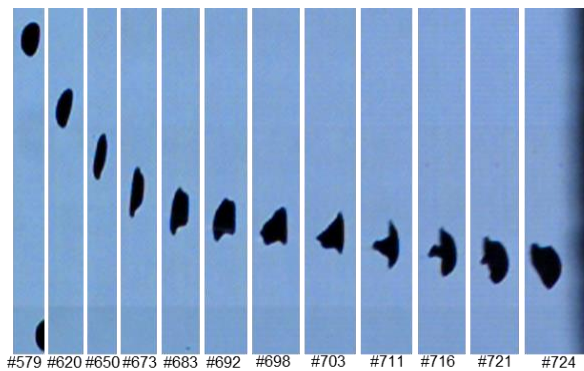**Figure 8.** Droplet Evolution Images. Run 101: Droplet Diameter 1mm, Model Velocity 40m/s. Corresponding Frames are under each image. The acquisition rate was 45000 fps.

Figure 9 shows the evolution of the droplet deformation and breakup for a droplet of 1 mm and model velocity of 50 m/s (case #7). It can be observed that the droplet follows a similar evolution as in case #6 up to frame #711 (Fig. 9). In case #6 at this point (frame #2072 in Fig. 6), the droplet impinged the model, however in case #7 the droplet breakup continues. The front part of the droplet seems to suffer a shear through the back (frame #716) and then the front part stars to resemble a hat where it appears an initiation of a cup.

Figure 9. Droplet Evolution Images. Run 102: Droplet Diameter 900μm, Model Velocity 50m/s. Corresponding Frames are under each image. The acquisition rate was 45000 fps.
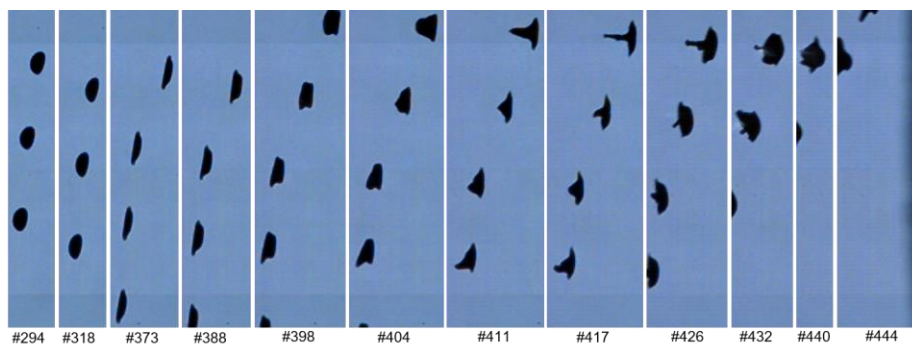

Figure 10. Droplet Evolution Images. Run 103: Droplet Diameter 1000μm, Model Velocity 60m/s. Corresponding Frames are under each image. The acquisition rate was 45000 fps.

Finally, Fig. 10 shows the droplet breakup evolution for droplets of 1 mm and model velocity of 60 m/s (case #8). The droplet evolves similar to case #7 up to frame #426 (see second droplet in Fig.10). Then the cup of the front hat that had appeared seems to suffer a shear through the back colliding in the centre (see frame # 440) as happened before (Fig. 8). Unfortunately, the droplet went out of the recording field of view and the final stage when the model appeared was not observed.
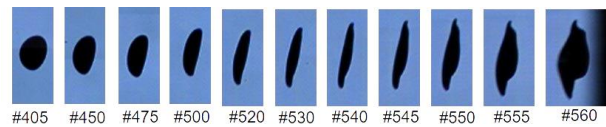

Figure 11. Droplet Evolution Images. Run 108: Droplet Diameter 1500µm, Model Velocity 30m/s. Corresponding Frames are under each image. The acquisition rate was 30000 fps.
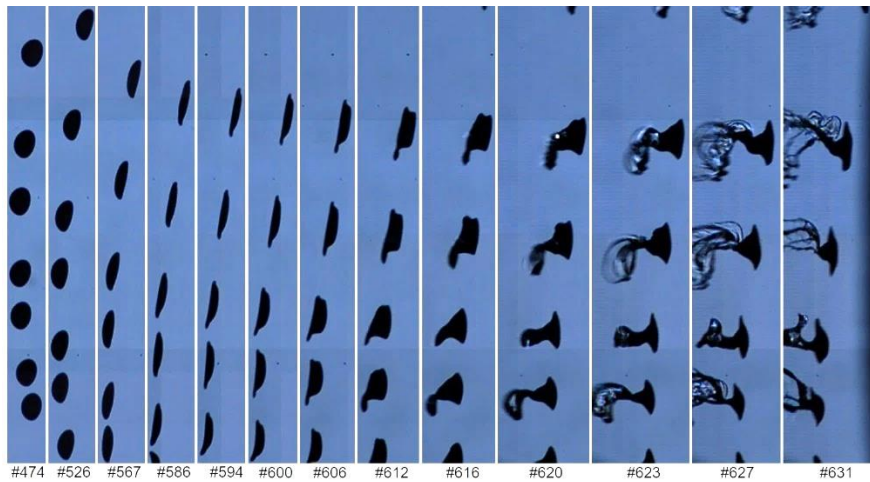

Figure 12. Droplet Evolution Images. Run 109: Droplet Diameter 1500µm, Model Velocity 40m/s. Corresponding Frames are under each image. The acquisition rate was 30000 fps.
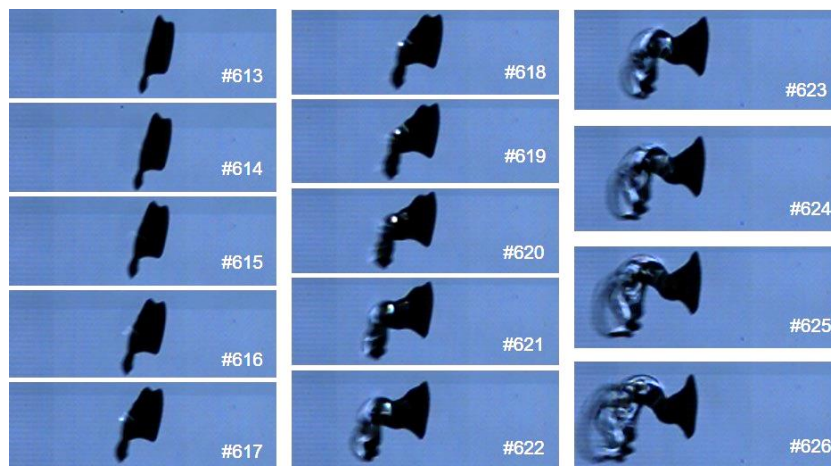

Figure 13. Droplet Evolution Images. Run 109: Droplet Diameter 1500µm, Model Velocity 40m/s. Corresponding Frames are under each image. The acquisition rate was 30000 fps.

For bigger droplets, whose diameters are on the order of 1500 µm, the droplet deformation and breakup evolution are displayed in Figs. 11, 12, 14 and 15 for model velocities of 30 m/s (case #9), 40 m/s (case #10), 50 m/s (case #11) and 60 m/s (case #12) respectively. For 30 m/s (case #9, see Fig.11), droplets deform as an oblate spheroid and then a bulge appear in the front part. For 40 m/s (case #10, see Fig. 12), after the bulge had emerged in the front part (frame #612), an asymmetry appeared (frame #620). Due to the bigger droplet size, asymmetries are more likely to occur. It seems that the rear part suffered a shear backstream and tried to collide as in smaller droplets (cases #6, #7 and #8), however, a bag is formed in the rear part (frame #623) that increases (frame #627). More details of the evolution are shown in Fig. 13, where frames from #616 to #626 are shown. Similar evolutions were observed for model velocities of 50 m/s (case #11, see Fig.14) and 60 m/s (case #12, see Fig.15).
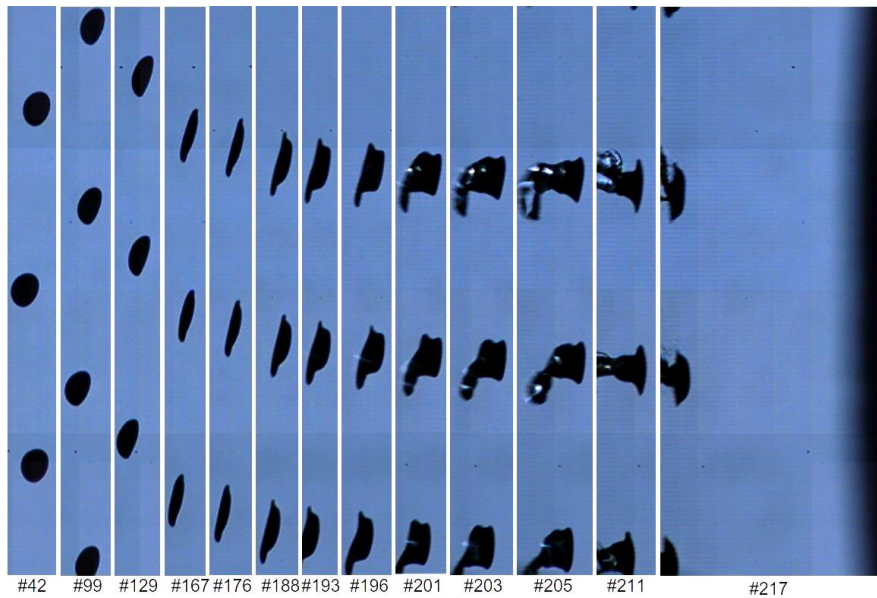
Figure 14. Droplet Evolution Images. Run 110: Droplet Diameter 1310µm, Model Velocity 50m/s. Corresponding Frames are under each image. The acquisition rate was 30000 fps.
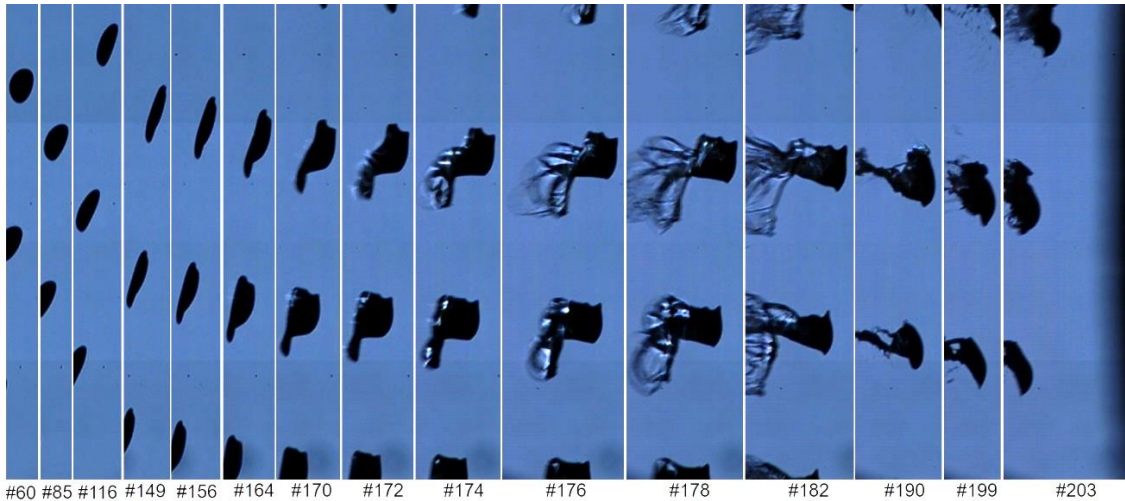

Figure 15. Droplet Evolution Images. Run 111: Droplet Diameter 1800µm, Model Velocity 60m/s. Corresponding Frames are under each image. The acquisition rate was 30000 fps.
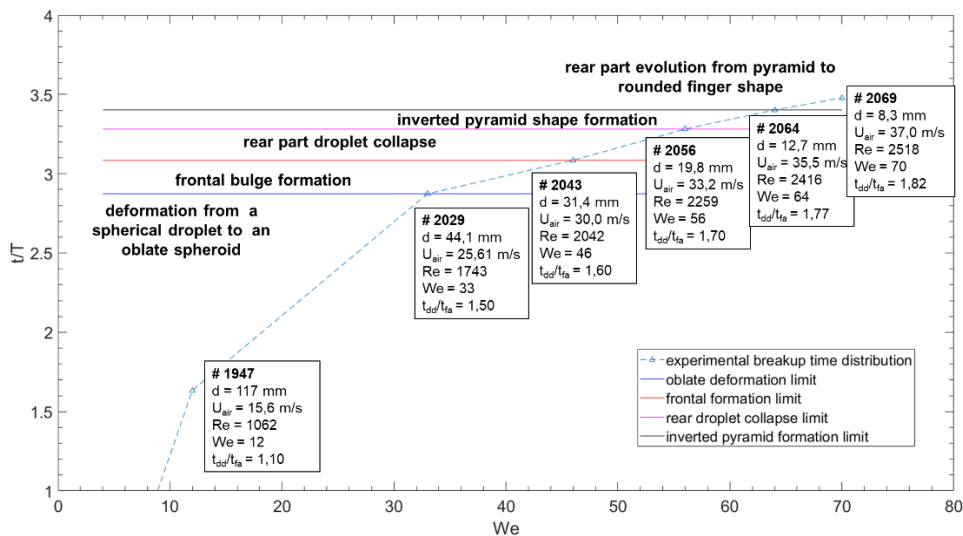

Figure 16. Breakup time distribution at different stages in the Run 101: Droplet Diameter 1mm, Model Velocity 40m/s. t/T is the ratio between time evolution and characteristic break up time defined as $T = D/\overline{U}_{air} \, (\rho_{air}/\rho_{et})^{0.5}$

Conclusions

The deformation and breakup evolution of ethyl alcohol droplets in a continuously accelerated flow field generated by a moving airfoil of chord 1.05m that approaches the droplets at velocities up to 60m/s have been investigated for droplets of diameters of 0.5 mm, 1 mm and 1.5 mm. Visualization of the droplet breakup has been obtained both with shadowgraph images taken by a high speed camera and using direct illumination and a high resolution camera. For droplets of 0.5 mm, only a slightly deformation was found for higher model velocities. However, a new type of breakup has been encountered for ethyl alcohol droplets of 1mm of diameter. After the deformations as an oblate spheroid, a bulge appears in the front part as in bag and stamen and it resemble the shape of a hat. However, then, instead of forming the bag, all the rear part of the droplet seems to collapse inside the droplet and a stamen is formed in the rear part of the droplets that grows a high quantity. At the same time, the droplet front part layer seems to shear back. A chart its provided in Fig. 16, so droplet evolution can be compared with other authors results for constant velocity air flows, as can be found in Cao et al. [18] and Jain et al. [19]. For the biggest droplets of diameter of 1.5 mm, droplets evolve first as an oblate spheroid and then a bulge appears in the front part resembling a hat. The outside cup of the hat seems to go downstream when an asymmetry occurs and at one side a bag is formed in the rear part that increases.

Acknowledgements

Nomenclature

d	distance to the model [mm]
ρ_{air}	air density [kg/m^3]
ρ_{et}	ethyl alcohol density [kg/m^3]
σ	surface tension ethyl alcohol-water [N/m]
D	droplet diameter [μm]
U_{air}	air velocity [m s^{-1}]
U_m	model velocity [m s^{-1}]
x	horizontal model coordinate [m]
y	vertical model coordinate [m]

References

[1] Wierzba, A., Takayama, K., 1988, AIAA Journal, 26(11), pp. 1329-1331
[2] Hsiang, L.P., and Faeth, G. M., 1992, International Journal of Multiphase Flow, 18(5), pp. 635-652.
[3] Luxford, G., Hammond, W., and Ivey, P., January 2005, 43rd Aerospace Sciences Meeting and Exhibit.
[4] Wierzba, A., 1990, Experiments in Fluids, 9, pp. 59-64.
[5] Theofanous, T. G., and Li, G.J., 2008, Physics of Fluids, 20, 052103 pp:1-14
[6] Guildenbecher, D. R., Lopez-Rivera, C., and Sojka, P. E., 2009, Experiments in Fluids, 46(3), pp. 371-402.
[7] Theofanous, T. G., 2011, Annual Review of Fluid Mechanics, 43, pp. 661-690
[8] Pilch, M., and Erdman, C. A., 1987, International Journal of Multiphase Flow, 13(6), pp. 741-757.
[9] Journal G., Houas L., Igra, O., Estivalez, J.-L., Devals, C., Meshkow, E. E., 2007, Proceeding of Real Society A, 463, pp. 3323-3345.
[10] Igra, O., Takayama, K., 1993, Proceeding of Real Society A, 442, pp. 231-247.
[11] Temkin, S., Metha, H. K., 1982, Journal of Fluid Mechanics, 116, pp. 297-312.
[12] Sor, S., Garcia-Magariño, A., Velazquez, A. 2016 Aerospace Science and Technology 58, pp 26-35
[13] Shao, S., Luo, K., and Fan, J., 2017 Chemical Engineering Journal 308 (2017) 619-631
[14] Garcia-Magariño, A., Sor, S., and Velazquez, A. 2015, Aerospace Science and Technology, 45, pp. 190-500.
[15] Garcia-Magariño, A., Sor, S., and Velazquez, A. 2017, ILASS–Europe 2017, 28th Conference on Liquid Atomization and Spray Systems,6-8 September 2017, Valencia, Spain. Paper 4991
[16] Garcia-Magariño, A., Sor, S., and Velazquez, A. 2017, ICLASS 2018, 14th Triennial International Conference on Liquid Atomization and Spray Systems, Chicago, IL, USA, July 22-26, 2018.
[17] Guidelbencher, D. R., Gao, J., Chen, J. and Sojka, P. E., 2017, International Journal of Multiphase Flow 94, pp 107-122.
[18] Cao, X. K., Sun, Z. G., Li, W. F., Liu, H. F., & Yu, Z. H., 2007,*Physics of Fluids*, *19*(5), pp 057103.
[19] Jain, M., Prakash, R. S., Tomar, G., & Ravikrishna, R. V., 2015, Proceedings of the Royal Society A,471(2177), pp 20140930.